Crossover from retro to specular Andreev reflections in bilayer graphene

Dmitri K. Efetov[1] and Konstantin B. Efetov[2,3]
[1]*Department of Electrical Engineering and Computer Science, Massachusetts Institute of Technology, Cambridge, Massachusetts 02142, USA*
[2]*Theoretische Physik III, Ruhr-Universität Bochum, D-44780 Bochum, Germany*
[3]*National University of Science and Technology "MISiS", Moscow 119049, Russia*
(Received 15 May 2016; revised manuscript received 17 July 2016; published 2 August 2016)

Ongoing experimental progress in the preparation of ultraclean graphene/superconductor (SC) interfaces enabled the recent observation of specular interband Andreev reflections (ARs) at bilayer graphene (BLG)/$NbSe_2$ van der Waals interfaces [Efetov *et al.*, Nat. Phys. **12**, 328 (2016)]. Motivated by this experiment we theoretically study the differential conductance across a BLG/SC interface at the continuous transition from high to ultralow Fermi energies E_F in BLG. Using the Bogoliubov-de Gennes equations and the Blonder-Tinkham-Klapwijk formalism we derive analytical expressions for the differential conductance across the BLG/SC interface. We find a characteristic signature of the crossover from intraband retro (high E_F) to interband specular (low E_F) ARs that manifests itself in a strongly suppressed interfacial conductance when the excitation energy $|\varepsilon| = |E_F| < \Delta$ (the SC gap). The sharpness of these conductance dips is strongly dependent on the size of the potential step at the BLG/SC interface U_0.

DOI: 10.1103/PhysRevB.94.075403

I. INTRODUCTION

Andreev reflections [1] (ARs) at normal metal (N) to superconductor (SC) interfaces describe the nontrivial conversion of a normal dissipative current into a dissipationless supercurrent. When an electron from N is injected onto a SC with an excitation energy $|\varepsilon| < \Delta$ (the SC gap), it is reflected back as a hole with an exactly opposite direction of motion. This perfect retroreflection process is understood as the result of the quasielasticity and momentum conservation of the process, combined with the fact that the hole has a negative mass. This picture is, however, only an approximation [2]. Due to a small energy loss of the electron due to its condensation into a Cooper pair, the holes energy and in-plane momentum, and hence its angle of reflection, are in all generality smaller than that of the incident electron. This effect is exceedingly small in typical metallic systems where E_F strongly exceeds typical energies of Δ, and perfect retro-AR in these systems has been confirmed in great detail [3].

Recent experimental efforts, however, shifted towards more exotic materials such as semiconductors [4], topological insulators [5], quantum Hall systems [6], carbon nanotubes [7], and graphene [8,9]. Unlike typical metals, these can have much lower E_F where the retroreflection process can be dramatically altered. Single-layer graphene (SLG) and bilayer graphene (BLG) [10,11], with their semimetallic band structure and the continuous gate tunability of E_F, are uniquely suited to study the E_F dependence of ARs at the crossover from large to arbitrarily small E_F. In the recently achieved regime where $|E_F| < \Delta$ [9], the reflected hole can undergo an interband transition from the conduction into the valence band, causing the hole's mass to change its sign. Under these conditions, energy and momentum conservation dictate that the reflection angle becomes a nontrivial function of E_F, resulting in a specular AR process for $E_F = 0$, where the angle of incidence and reflection are equal, $\alpha = \alpha'$ [Figs. 1(a) and 1(b)].

In this paper we work out a detailed analytical description of the differential conductance across a BLG/SC interface at the continuous transition from high $|E_F| \gg \Delta$ to low $|E_F| < \Delta$ Fermi energies. While direct measurements of scattering angles are experimentally challenging, measurements of a nonlinear conductance $G_{NS}(\varepsilon)$ as a function of the excitation energy ε are easily experimentally approachable and can illuminate the underlying scattering processes at the N/SC interface. We find two distinct regimes for $|\varepsilon| < |E_F|$ and $|\varepsilon| > |E_F|$ where intraband retroreflections and interband specular reflection are taking place, respectively. We identify conductance dips in $G_{NS}(\varepsilon)$ at the energy condition $|\varepsilon| = |E_F|$, where the hole is reflected onto the charge neutrality point. This line in the energy phase space separates the two distinct regimes, so marking the crossover from retro intraband to specular interband AR.

II. MODEL AND METHOD

We model the BLG/SC junction considering a setup similar to the one presented in the experimental device of Ref. [9] and similar to the one used in the theoretical model in Ref. [2] [Fig. 1(a)]. We assume an impurity free BLG sheet in the half plane $x > 0$ that has an ideal electrical contact with a SC lead at $x < 0$. The SC is modeled by a BLG sheet with an induced SC gap $\Delta(x)$ that appears due to the SC proximity effect. For a more realistic BLG/SC interface we also assume that the SC contact induces an additional potential $U(x)$ due to work function matching of the BLG and the SC, as it is typically observed for all graphene/metal interfaces. Assuming that only s-wave singlet SC is induced and that only electrons of different valleys form Cooper pairs in the BLG, we write the Bogoliubov-de Gennes (BdG) equations [12] that describe the electron motion in the system in the standard form,

$$\begin{pmatrix} \mathcal{H}(\hat{\mathbf{K}},x) - E_F & \Delta(x) \\ \Delta^*(x) & E_F - \mathcal{H}(\hat{\mathbf{K}},x) \end{pmatrix} \begin{pmatrix} u \\ v \end{pmatrix} = \varepsilon \begin{pmatrix} u \\ v \end{pmatrix}, \quad (2.1)$$

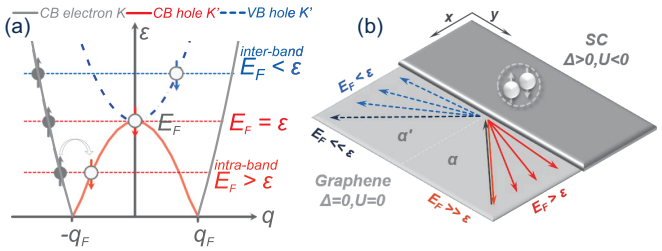

FIG. 1. (a) Excitation spectrum $\varepsilon(q)$ for a fixed $E_F < \Delta$. With an increasing excitation voltage ε, the momentum in the y direction q of the reflected hole continuously increases from negative to positive values, passing through zero when $E_F = \varepsilon$. (b) Schematics of the reflection angles of AR holes in the various energy limits. Starting from perfect intraband retroreflection in the high E_F limit, the reflection angle α' continuously increases towards $\pi/2$ as E_F is lowered. At the crossover point separating intraband and interband ARs, $E_F = \varepsilon$, α' exhibits a jump to $-\pi/2$, which eventually results in perfect interband specular reflection $\alpha = \alpha'$ when $E_F = 0$.

where

$$\mathcal{H}(\hat{\mathbf{K}},x) = \mathcal{H}_0(\hat{\mathbf{K}}) + U(x) \tag{2.2}$$

and $\hat{\mathbf{K}}$ is the momentum operator. The electron and hole wave functions u and v denote the amplitudes of the four different atoms in the BLG unit cell $u = (u_{A1},u_{A2},u_{B2},u_{B1})$ and $v = (v_{A1},v_{A2},v_{B2},v_{B1})$, where A,B stand for two sublattice sites and 1,2 numerate the layers.

The Hamiltonian $\mathcal{H}_0(\mathbf{K})$ of the normal BLG for one valley is written as a 4×4 matrix [13–15],

$$\mathcal{H}_0(\mathbf{K}) = \hbar v \begin{pmatrix} 0 & Ke^{i\alpha} & -t_\perp & 0 \\ Ke^{-i\alpha} & 0 & 0 & 0 \\ -t_\perp & 0 & 0 & Ke^{-i\alpha} \\ 0 & 0 & Ke^{ia} & 0 \end{pmatrix}, \tag{2.3}$$

where $\alpha(\mathbf{K}) = \arctan(q/k)$ and $K = \sqrt{k^2+q^2}$ (q is the y component and k is the x-component of $\mathbf{K}$). Writing Eq. (2.3), we imply that the corresponding four-component wave functions are chosen in the form $\Psi = (\Psi_{A1},\Psi_{A2},\Psi_{B2},\Psi_{B1})$.

At the BLG/SC interface ($x = 0$) we assume a sharp potential step of $U(x)$ and $\Delta(x)$:

$$U(x) = \begin{cases} -U_0, & x < 0, \\ 0, & x > 0, \end{cases} \tag{2.4}$$

$$\Delta(x) = \begin{cases} \Delta_0 e^{i\phi}, & x < 0, \\ 0, & x > 0. \end{cases} \tag{2.5}$$

This potential profile is clearly an oversimplification, since in the experiment these quantities can scale rather smoothly at the interface. While our assumption may result in a certain overestimation of the transmission amplitude at the interface, we do not think that the dependence of the conductance on E_F and ε can essentially be different for a smoothed potential step, and we believe that this approximation should not change the basic picture of the conversion from retro to specular ARs.

In accordance with the experimentally known parameters, we assume that the potential U_0 is larger than the energies E_F, Δ_0, and ε but that the largest energy in BLG is the coupling energy $\hbar v t_\perp$ between the layers. Therefore, we use the inequalities

$$\hbar v t_\perp \gg U_0 \gg E_F, \Delta_0, \varepsilon. \tag{2.6}$$

Here we want to specifically point out that the inequalities (2.6) are different from those used in Ref. [16], where it was assumed that $U_0 \gg \hbar v t_\perp$. We particularly use the opposite limit in our calculation to match experimentally available parameters, where typically the interlayer coupling energy is significantly bigger than the potential step region of the parameters ε and E_F.

One can calculate the differential conductance $G_{NS}(\varepsilon)$ for $|\varepsilon| < \Delta_0$ and $T = 0$ by considering the scattering of particles that are moving from right to left. Following the formalism of Ref. [17], one can solve Eqs. (2.1)–(2.6) separately for $x > 0$ and $x < 0$, then match these solutions at $x = 0$ and so find the normal reflection $r(\varepsilon,\alpha)$ and Andreev reflection $r_A(\varepsilon,\alpha)$ amplitudes for all incidence angles α,

$$\frac{G_{NS}(\varepsilon)}{G_{NN}(\varepsilon)} = \int_0^{\pi/2} \left[1 - r^2(\varepsilon,\alpha) + r_A^2(\varepsilon,\alpha)\right] \cos\alpha d\alpha, \tag{2.7}$$

where $G_{NN}(\varepsilon)$ is the differential conductance across the interface of two normal BLG sheets.

Such a calculation is not very difficult for SLG [2]; however, a corresponding calculation for BLG is considerably more cumbersome and it is not easy to obtain explicit formulas in all regions of the variables ε and E_F. Here we follow Beenakkers approach [18], which allows one to express the conductance $G_{NS}(\varepsilon)$ in terms of transmission $t(\varepsilon)$ and reflection $r(\varepsilon)$ amplitudes of the scattering on the interface between two normal metals, by simply putting $\Delta_0 = 0$. This approach works only within the mean-field requirement of SC, where it is required that $\Delta_0 \ll E_F + U_0$, which assures that the SC coherence length is large compared to the Fermi wavelength in the SC. We write the differential conductance $G_{NS}(\varepsilon)$ in the form

$$G_{NS}(\varepsilon) = \frac{4e^2}{h} \mathrm{Tr}[m(\varepsilon)m^+(\varepsilon)], \tag{2.8}$$

with

$$m(\varepsilon) = t_{12}(\varepsilon)[1 - e^{-2i\beta} r_{22}^*(-\varepsilon) r_{22}(\varepsilon)]^{-1} t_{21}^*(-\varepsilon), \tag{2.9}$$

where $\beta = \arccos(\varepsilon/\Delta_0)$.

The conductance $G_{NN}(\varepsilon,E_F)$ across two normal regions 1 and 2 reads

$$G_{NN}(\varepsilon,E_F) = \frac{4e^2}{h} \mathrm{Tr}|t_{12}(\varepsilon,E_F)|^2, \tag{2.10}$$

where regions 1 and 2 correspond to N ($x > 0$) and SC ($x < 0$), respectively. In other words, Eqs. (2.8)–(2.10) show that calculating the transmission $t_{12}(\varepsilon),t_{21}(\varepsilon)$ and reflection $r_{12}(\varepsilon),r_{21}(\varepsilon)$ amplitudes (see the Appendix) for right- and left-moving particles at the interface one obtains the differential conductance $G_{NS}(\varepsilon)$ of the BLG/SC interface. The trace Tr over the scattering channels in Eqs. (2.8) and (2.10) reduces to the integration over the momentum q parallel to the interface. Equations (2.8)–(2.10) also demonstrate that, in order to calculate the differential conductance G_{NS}, it is enough to understand the scattering on the interface between two normal metals, which is a considerably simpler task than calculating the differential conductance using the original formula (2.7).

Generally, one can see from Eqs. (2.8) and (2.9) an important difference between the conductance of SLG and that of BLG. For SLG the energy spectrum follows the Dirac equations and hence the transmission amplitude for an electron is of order one for any U_0 due to the so-called Klein effect. On the contrary, the spectrum of BLG is approximately quadratic and one can conclude by using standard formulas [19] for scattering on a step function that the transmission amplitude $t_{12}(\varepsilon)$ decays proportionally to $U_0^{-1/2}$ at large U_0 and therefore is very small. For this reason, while the conductance G_{NN} in BLG is proportional to t^2, the conductance G_{NS} is proportional to t^4 and hence can be much smaller than G_{NN}. The presence of the SC gap can therefore strongly reduce the conductance across the interface.

In the next section we present the main analytical formulas for the conductance, leaving details of the derivation for the Appendix.

III. ANALYTICAL EXPRESSIONS FOR THE DIFFERENTIAL CONDUCTANCE

We have to specifically distinguish between two distinct regimes:

(A) $|\varepsilon| < |E_F|$, the reflected hole has positive energy (conduction band) and negative mass $\Rightarrow$ intraband retroreflection;

(B) $|\varepsilon| > |E_F|$, the reflected hole has negative energy (valence band) and positive mass $\Rightarrow$ interband specular reflection.

A. $G_{NS}(\varepsilon)$ for $|\varepsilon| < |E_F|$ (retroreflection)

Equations (2.8)–(2.10) can be rewritten using the integration over the longitudinal component q of the momentum instead of the trace over the transversal channels. However, it is even more convenient to integrate over the incident angle α. The angle α corresponds to the energy ε, while the reflection angle α' corresponds to the energy $-\varepsilon$. These angles are related to each other by the condition that q is conserved during the reflection process and, therefore,

$$\frac{\sin\alpha'}{\sin\alpha} = -\sqrt{\frac{E_F+\varepsilon}{E_F-\varepsilon}}. \tag{3.1}$$

From this relation one can conclude that Andreev reflections are possible for the angles $|\alpha| < \alpha_c$, where

$$\alpha_c = \arcsin\sqrt{\frac{E_F-\varepsilon}{E_F+\varepsilon}}. \tag{3.2}$$

Writing

$$\Phi(\alpha) = \arcsin(\sin^2\alpha), \tag{3.3}$$

$$\Phi(\alpha') = \arcsin(\sin^2\alpha') = \arcsin\left[\left(\frac{E_F+\varepsilon}{E_F-\varepsilon}\right)\sin^2\alpha\right], \tag{3.4}$$

the conductance G_{NS} can be reduced to the form

$$G_{NS}(\varepsilon) = 2G_0K_0(\varepsilon)\int_0^{\alpha_c}\frac{Y_\varepsilon(\alpha,\alpha')\cos\alpha}{2|X_\varepsilon(\alpha,\alpha')|^2}d\alpha, \tag{3.5}$$

where

$$\begin{aligned} Y_\varepsilon(\alpha,\alpha') &= |t_{21}(\varepsilon)|^2|t_{21}(-\varepsilon)|^2 \\ &= 16L(\varepsilon)L(-\varepsilon)\cos\alpha\cos\alpha'(1+\sin^2\alpha)(1+\sin^2\alpha'), \end{aligned} \tag{3.6}$$

$$L(\varepsilon) = \sqrt{\frac{|\varepsilon+E_F|}{U_0}} \ll 1, \tag{3.7}$$

and

$$K_0(\varepsilon) = \sqrt{|\varepsilon+E_F|t_\perp/\hbar v}. \tag{3.8}$$

The function $X_\varepsilon(\alpha,\alpha')$ entering Eq. (3.5) equals

$$X_\varepsilon(\alpha,\alpha') = \tfrac{1}{2}[1-e^{-2i\beta}r_{22}^*(-\varepsilon)r_{22}(\varepsilon)], \tag{3.9}$$

where β is given by the expression

$$\beta = \arccos(\varepsilon/\Delta_0). \tag{3.10}$$

Approximating this function by lowest orders in $L(\varepsilon)$ we write

$$\begin{aligned} |X_\varepsilon(\alpha,\alpha')|^2 &= \sin^2\beta - 2\sin\beta\{L(\varepsilon)\sqrt{1+\sin^2\alpha}\sin[\beta+\Phi(\alpha)] + L(-\varepsilon)\sqrt{1+\sin^2\alpha'}\sin[\beta-\Phi(\alpha')]\} + L^2(\varepsilon)(1+\sin^2\alpha) \\ &\quad + L^2(-\varepsilon)(1+\sin^2\alpha') + 2L(\varepsilon)L(-\varepsilon)\sqrt{(1+\sin^2\alpha)(1+\sin^2\alpha')}\{\cos[2\beta-\Phi(\alpha')+\Phi(\alpha)] - 2\sin\Phi(\alpha)\sin\Phi(\alpha')\}. \end{aligned} \tag{3.11}$$

The quadratic terms in $L(\varepsilon), L(-\varepsilon)$ have been kept in $|X_\varepsilon(\alpha,\alpha')|^2$ because they are the only contributions that do not vanish at $\beta \to 0$. In principle, there are also quadratic terms proportional to $\sin\beta$, but they can be neglected.

B. $G_{NS}(\varepsilon)$ for $|\varepsilon| > |E_F|$ (specular reflection)

In this case the angles α and α' are related to each other as

$$\frac{\sin\alpha'}{\sin\alpha} = \sqrt{\frac{\varepsilon+E_F}{\varepsilon-E_F}} \tag{3.12}$$

and the critical angle α_c equals to

$$\alpha_c = \arcsin\sqrt{\frac{\varepsilon-E_F}{\varepsilon+E_F}}. \tag{3.13}$$

For $\Phi(\alpha)$ we have the same relation as in Eq. (3.3) and obtain for $\Phi(\alpha')$

$$\Phi(\alpha') = \arcsin\left[\left(\frac{\varepsilon+E_F}{\varepsilon-E_F}\right)\sin^2\alpha\right]. \tag{3.14}$$

The conductance $G_{NS}(\varepsilon)$ is then determined as before by Eq. (3.5). For the function $Y_\varepsilon(\alpha,\alpha')$ we therefore have

$$Y_\varepsilon(\alpha,\alpha') = |t_{21}(\varepsilon)|^2|t_{21}(-\varepsilon)|^2 = 16L(\varepsilon)L(-\varepsilon)\cos\alpha(1+\sin^2\alpha)\cos\alpha'\sin^2\alpha'. \tag{3.15}$$

The function $X_\varepsilon(\alpha,\alpha')$ is determined from Eq. (3.9) and we obtain

$$|X_\varepsilon(\alpha,\alpha')|^2 = \sin^2\beta - 2\sin\beta\{L(\varepsilon)\sqrt{1+\sin^2\alpha}\sin[\beta+\Phi(\alpha)] - L(-\varepsilon)\cos\alpha'\cos[\beta+\Phi(\alpha')]\} + 2L(\varepsilon)L(-\varepsilon) \times\sqrt{1+\sin^2\alpha}\cos\alpha'\{\sin[2\beta+\Phi(\alpha)+\Phi(\alpha')] - 2\cos\phi(\alpha)\sin\Phi(\alpha')\} + L^2(\varepsilon)(1+\sin^2\alpha) + L^2(-\varepsilon)\cos^2\alpha'. \tag{3.16}$$

C. Conductance G_{NN} of the interface between two normal metals

The transmission amplitude $t_{12}(\varepsilon)$ determines the zero-temperature conductance $G_{NN}(\varepsilon)$ between two normal metals entering Eq. (2.10). At a fixed E_F the conductance $G_{NN}(\varepsilon)$ is given by the following formula:

$$G_{NN}(\varepsilon) = G_0K_0(\varepsilon)\int_{-\pi/2}^{\pi/2}|t_{12}(\varepsilon)|^2\cos\alpha d\alpha. \tag{3.17}$$

The final form of the conductance $G_{NN}(\varepsilon)$ between the normal metals can be written as

$$G_{NN}(\varepsilon) = G_0K_0(\varepsilon)\int_{-\pi/2}^{\pi/2}4L(\varepsilon)\cos^2\alpha(1+\sin^2\alpha)d\alpha = \frac{5\pi}{2}G_0K_0(\varepsilon)L(\varepsilon). \tag{3.18}$$

The formulas presented in this section describe the conductances for all parameters of interest and one can explicitly compare the corresponding numerical curves with experimental results. All the details of the derivation of the results of the present section can be found in the Appendix.

IV. NUMERICAL STUDY AND DISCUSSION

In the AR process the incident electron has a total energy of $E_F+\varepsilon$ and condenses into a Cooper pair with a total energy of $2E_F$ after transmission into the SC. Here energy conservation dictates that the reflected hole has a slightly lower total energy of $E_F-\varepsilon$. This energy loss of 2ε can have dramatic consequences for an ultralow E_F, where for the condition $|\varepsilon|>E_F$, the incident conduction hole electron can be reflected as a hole in the valence band [Figs. 1(a) and 1(b)].

Due to momentum conservation parallel to the interface q, the reduced energy of the hole directly translates into an altered angle of reflection α' as compared to the angle of incidence α. As was shown in the previous section, these angles are related to each other by the simple relation (3.1), from which one can conclude that ARs are possible only for angles $\alpha<\alpha_c$, where α_c [Eq. (3.2)] plays the role of the angle of total internal reflection for ARs and is plotted in Fig. 2(a) for various fixed E_F. As can be seen from the plots, for $\varepsilon=0$, $\alpha_c=\pi/2$, and ARs are possible for all angles of incidence. However, when $\varepsilon=E_F$, $\alpha_c=0$, and ARs are prohibited for all angles.

The explicit analytical formula for G_{NS}, Eq. (3.5), and subsequent formulas for the functions entering this equation allow us to numerically calculate $G_{NS}(\varepsilon,E_F)$ for the full phase space. Here we explicitly calculate the normalized conductance, $G_{NS}(\varepsilon,E_F)/G_{NN}(\varepsilon,E_F,T)$, since this allows to better highlight the conductance features that arise solely from the SC proximity effect. As both G_{NS} and G_{NN} in a realistic sample are generally subjected to effect of energy fluctuations and disorder, one can eliminate these undesired and hard-to-quantify effects by simply dividing these out. Since measurements of the SC state are typically performed at $T\ll T_c$ [9], one can use $G_{NS}(\varepsilon,E_F)$ at $T=0$, with a reasonable accuracy. However, we specifically derive a temperature broadened form of $G_{NN}(\varepsilon,E_F,T)$ since in an experiment one can only obtain this quantity at elevated temperatures $T>T_c$,

$$G_{NN}(\varepsilon,E_F,T) = \frac{5\pi}{4}\int_{-\infty}^{\infty}\frac{K_0(\varepsilon)L(\varepsilon)dE_F}{4T\cosh^2\left(\frac{E_F-\varepsilon}{2T}\right)}. \tag{4.1}$$

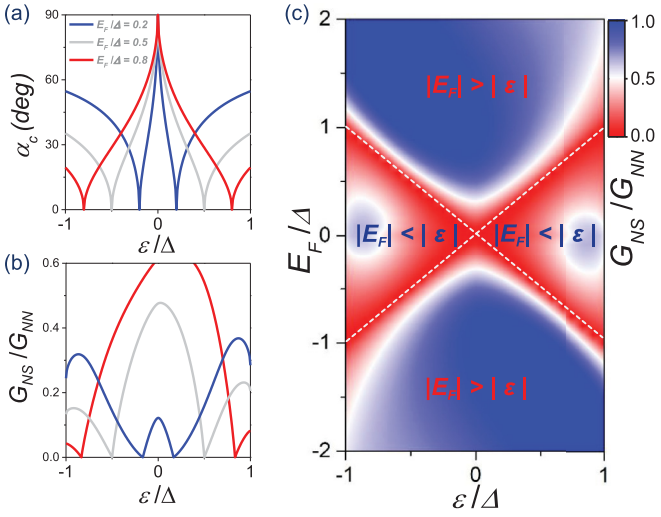

FIG. 2. (a) Angle of total internal reflection for ARs α_c for various fixed E_F. For $\varepsilon=0$, $\alpha_c=\pi/2$, and ARs are possible for all angles of incidence. For $\varepsilon=E_F$, ARs are prohibited for all angles and $\alpha_c=0$. (b) Conductance $G_{NS}/G_{NN}(10K)$ as a function as a function of ε for the same E_F as in (a). The conductance is pinched off at same positions at which $\alpha_c=0$. (c) Two-dimensional color map of $G_{NS}/G_{NN}(10K)$ for a function of both ε and E_F . The conductance dips scale along the diagonal lines defined by the condition $|\varepsilon|=|E_F|$ and define a phase diagram that separates the map into regions of retro and specular ARs. Here we used the parameter $U_0=5$ meV.

In Fig. 2(b) we plot out $G_{NS}/G_{NN}(10K)$ (here we choose $T = 10$ K for G_{NN} as was used in Ref. [9]) as a function of ε for various fixed E_F. Since $\alpha_c = 0$ for $|\varepsilon| = |E_F|$, it can be seen from Eq. (3.5) that the conductance vanishes, $G_{NS} = 0$, at these points. As discussed earlier, this condition coincides exactly with the condition that separates intraband retro from interband specular reflections. The depleted interfacial resistance for this energy condition marks therefore the crossover between the two different regimes and so provides a strong experimental observable. In Fig. 2(c) we plot a 2D color map of G_{NS}/G_{NN} for a function of both ε and E_F. The conductance dips scale along the diagonal lines defined by the condition $|\varepsilon| = |E_F|$ and define a striking crosslike shape. One can use this map as a phase diagram to separate the region of retro and specular ARs.

Here the slight asymmetry of G_{NS}/G_{NN} around $\varepsilon = 0$ and $E_F = 0$ arises only from the G_{NN} component of the normalized conductance, whereas the G_{NS} component is symmetric. This comes from a slight shift of E_F when ε is tuned, resulting in a diagonally changing position of the charge neutrality point. Here we want to specifically point out that our results for $U_0 = 5$ meV are quite different than those in Ref. [16], which were calculated assuming an exceedingly large $U_0 \gg \hbar v t_\perp$. In particular, we do not observe the sharp conductance dips around $\epsilon/\Delta \sim 1$ which were attributed to pseudospin properties in BLG in Ref. [16].

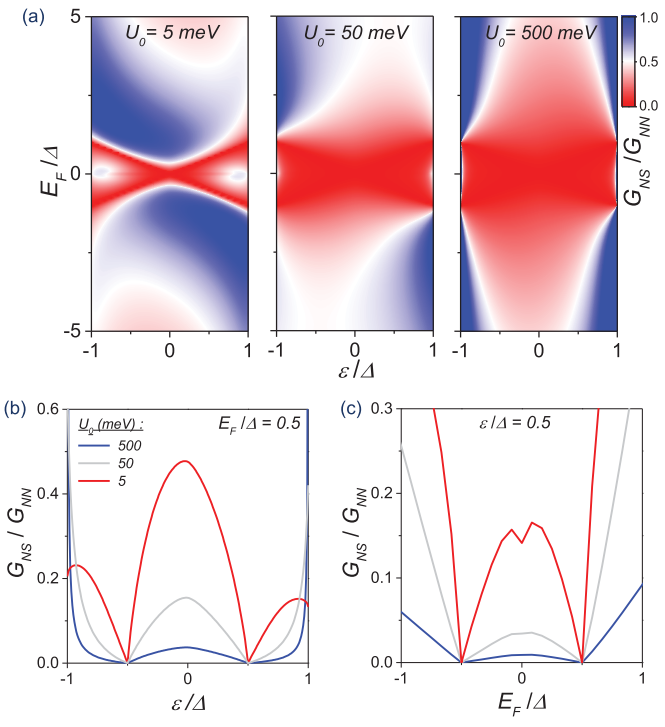

FIG. 3. Normalized conductance $G_{NS}/G_{NN}(10K)$ for three different values of the potential step at the N/SC interface U_0. As can be seen from the various graphs, the inner gap conductance is strongly reduced for higher values of U_0. This results in the strong suppression of the sharpness and contrast of the characteristic crossover point from retro to specular ARs, $E_F = \varepsilon$. (a) Two-dimensional color plots as a function of ε and E_F. (b) Excitation energy dependence ε for a fixed $|E_F| < \Delta$. (c) Fermi energy dependence E_F for a fixed $|\varepsilon| < \Delta$.

The integrand in Eqs. (2.8) and (3.5) contains only one unknown parameter, the potential step at the BLG/SC interface U_0 (in Fig. 2 we used a $U_0 = 5$ meV). In principle, this value can be found in the literature for various materials or can be extracted by fitting the experimental curves with the presented theory. In general, it is important to emphasize the role of U_0 for the purpose of experiments as it can strongly affect the outcome. In Fig. 3 we study the normalized conductance G_{NS}/G_{NN} for various values of U_0. One can see that the inner gap conductance is strongly reduced for higher values of U_0. This results in the strong suppression of the sharpness and contrast of the characteristic crossover point from retro to specular ARs, $E_F = \varepsilon$. This suppression can be explained by the previously discussed decaying transmission amplitude $t_{12}(\varepsilon)$, which scales proportionally to $U_0^{-1/2}$ and is therefore very small for large U_0. For experimental studies of specular AR in BLG/SC junctions it is therefore important to engineer an interface with a rather small potential step U_0.

V. CONCLUSIONS

In this paper we have rigorously worked out analytical expressions for the differential conductance across a BLG/SC interface for the ultimate limits of large and small Fermi energies E_F. We have found, that while for $E_F \gg \Delta$ the AR process is described by intraband retroreflections, in the limit of $E_F \ll \Delta$ they are described by interband specular reflections. From numerical calculations we find that the crossover between the two processes has a clear experimental signature that manifests itself in a strongly suppressed interfacial conductance when the excitation energy $|\varepsilon| = |E_F| < \Delta$.

ACKNOWLEDGMENTS

The authors thank C. W. J. Beenakker, P. Kim, and J. D. Pillet for helpful discussions. K. B. Efetov gratefully acknowledges the financial support of the Ministry of Education and Science of the Russian Federation in the framework of Increase Competitiveness Program of NUST "MISiS" (Grant No. K2-2014-015) and Priority Program No. 1459 "Graphene" of Deutsche Forschungsgemeinschaft.

APPENDIX A: EIGENENERGIES, WAVE FUNCTIONS, TRANSMISSION, AND REFLECTION AMPLITUDES IN THE ABSENCE OF A SC GAP

Equations (2.8)–(2.10) allow one to reduce the calculation of the conductance of the N/SC junction to study of the transmission and reflection amplitudes between two normal metals. This can be done putting $\Delta = 0$ in Eqs. (2.1)–(2.3) and writing the obtained equation in the form

$$[\mathcal{H}_0(\hat{\mathbf{K}}) + U(x)]u = Eu, \tag{A1}$$

with $U(x)$ defined in Eq. (2.4). One should now solve Eqs. (A1) separately at $x > 0$ and $x < 0$ and match the solutions at $x = 0$.

1. Eigenenergies

First, following Refs. [13–15], we write the eigenenergies $E(\mathbf{K})$ of the Hamiltonian $\mathcal{H}_0(\mathbf{K})$, Eq. (2.3), for an arbitrary

relation between $t_\perp$ and the characteristic energies inside one layer in the form

$$\begin{aligned} E_1(\mathbf{K}) &= \hbar v[-t_\perp/2 - \mathcal{E}(\mathbf{K})], \\ E_2(\mathbf{K}) &= \hbar v[-t_\perp/2 + \mathcal{E}(\mathbf{K})], \\ E_3(\mathbf{K}) &= \hbar v[t_\perp/2 + \mathcal{E}(\mathbf{K})], \\ E_4(\mathbf{K}) &= \hbar v[t_\perp/2 - \mathcal{E}(\mathbf{K})], \end{aligned} \tag{A2}$$

where

$$\mathcal{E}(\mathbf{K}) = \sqrt{(t_\perp/2)^2 + K^2}. \tag{A3}$$

Provided that the interlayer coupling $t_\perp$ exceeds all the other energies, the bands of the Hamiltonian (2.3) with the spectra $E_1(\mathbf{k})$ and $E_3(\mathbf{k})$ are far away from the Fermi energy and their contribution into physical quantities can be neglected. The eigenenergies of the first two low-energy bands take in the limit of small $|\mathbf{k}| \ll t_\perp$ the following form:

$$\begin{aligned} E_2(\mathbf{k}) &= \hbar v[-t_\perp/2 + \mathcal{E}(\mathbf{k})] \approx \frac{\hbar v K^2}{t_\perp}, \\ E_4(\mathbf{k}) &= \hbar v[t_\perp/2 - \mathcal{E}(\mathbf{k})] \approx -\frac{\hbar v K^2}{t_\perp}. \end{aligned} \tag{A4}$$

In Eq. (A4), $E_2(\mathbf{K})$ describes the conduction band and $E_4(\mathbf{K})$ describes the valence band. Using the inequality (2.6) we consider only these low-lying bands and no higher energy bands.

2. Wave functions

The Hamiltonian $\mathcal{H}_0(\mathbf{k})$, Eq. (2.3), can be diagonalized as was done in Ref. [15], and we can easily obtain four-component vectors u that satisfy the equation

$$[\mathcal{H}(\mathbf{k}) - E_F]u = \varepsilon u. \tag{A5}$$

Here we consider only the case $E_F > 0$. The solutions depend on the sign of $\varepsilon + E_F$ and we write them separately for $\varepsilon + E_F > 0$ and $\varepsilon + E_F < 0$.

For the low-lying eigenvalues we obtain

$$\varepsilon_2 = -E_F + \frac{\hbar v}{t_\perp} K^2, \tag{A6}$$

$$\varepsilon_4 = -E_F - \frac{\hbar v}{t_\perp} K^2. \tag{A7}$$

In order to calculate the wave functions one should choose an eigenvalue ε and determine K as a function of this ε. It is clear that constructing plane waves in the region of the normal metal N_1 and $E_F > 0$ one should take the solution of Eq. (A6) for K as a function of ε at $\varepsilon > -E_F$ and of Eq. (A7) at $\varepsilon < -E_F$. In addition, one has a solution for K of (A7) at $\varepsilon > -E_F$ and of (A6) at $\varepsilon < -E_F$. The latter solutions are either exponentially growing or decaying as functions of x. Nevertheless, they should also be taken into account when matching functions at the interface because we have the deep potential $-U_0$ at $x < 0$ and the exponential growth can change to the plane wave behavior there.

Here we calculate the wave functions for the region $x > 0$. These can be, however, also used in the region $x < 0$ after shifting the energy $E_F \to E_F + U_0$. We later denote all quantities where this shift has been done by adding the subscript U_0, thus obtaining $u^{R,L}_{1U_0}$, $u^{R,L}_{2U_0}$, etc.

a. Plane wave solutions at $\varepsilon + E_F > 0$

In this region of the energies we have left- and right-moving electrons of the conduction band and use Eq. (A6). The solution u_1^R for right-moving particles in this region takes the form

$$u_1^R = \frac{e^{ikx+iqy}}{2\sqrt{K_0/t_\perp \cos\alpha}} \begin{pmatrix} K_0/t_\perp \\ e^{-i\alpha} \\ K_0/t_\perp \\ e^{i\alpha} \end{pmatrix}, \tag{A8}$$

while the solution for the left-moving particles u_1^L reads [we use a compact notation $K_0 = K_0(\varepsilon)$, Eq. (3.8)]

$$u_1^L = \frac{e^{-ikx+iqy}}{2\sqrt{K_0/t_\perp \cos\alpha}} \begin{pmatrix} -K_0/t_\perp \\ e^{i\alpha} \\ -K_0/t_\perp \\ e^{-i\alpha} \end{pmatrix}. \tag{A9}$$

The wave functions u_1^R and u_1^L correspond to the eigenenergy $E_2(\mathbf{k})$, Eq. (A4), and belong to the conduction band. They are normalized assuming the current 1 along the x axis for the right-moving particles and -1 for left-moving ones. This fact can easily be checked using the matrix form of the current operator

$$\mathbf{j} = e\sigma \tag{A10}$$

having the x component

$$j_x = e\sigma_x, \tag{A11}$$

where σ is the vector of Pauli matrices in the sublattice space of graphene.

Having fixed $E_F > 0$ we have to express k and q in terms of K_0 and α. Since we introduced the angle α as

$$k - iq = K_0 e^{-i\alpha}, \tag{A12}$$

we obtain for $\varepsilon + E_F > 0$ the following relations for the variables α and k:

$$k = K_0 \cos\alpha, \quad q = K_0 \sin\alpha. \tag{A13}$$

Here the angle α varies in the interval $-\pi/2 < \alpha < \pi/2$.

b. Plane wave solutions at $\varepsilon + E_F < 0$

In this region of energies we have plane waves corresponding to right- and left-moving holes from the valence band and use Eq. (A7). For the right-moving holes we obtain the normalized wave functions

$$u_2^R = \frac{e^{ik'x+iqy}}{2\sqrt{K_0/t_\perp \cos\alpha'}} \begin{pmatrix} K_0/t_\perp \\ e^{-i\alpha'} \\ -K_0/t_\perp \\ -e^{i\alpha'} \end{pmatrix}, \tag{A14}$$

where

$$k' = -K_0 \cos\alpha', \quad q = -K_0 \sin\alpha'. \tag{A15}$$

In Eqs. (A14) and (A15), the angle α' varies in the interval $-\pi/2 < \alpha' < \pi/2$.

The opposite signs in Eq. (A15), as compared to Eq. (A13), are due to the fact that we now consider holes from the valence band instead of electrons from the conduction band.

The solution u_2^L for the left-moving particles takes the form

$$u_2^L = \frac{e^{-ik'x+iqy}}{2\sqrt{K_0/t_\perp \cos\alpha'}} \begin{pmatrix} -K_0/t_\perp \\ e^{i\alpha'} \\ K_0/t_\perp \\ -e^{-i\alpha'} \end{pmatrix}. \tag{A16}$$

The current of the right-moving holes (functions u_2^R) equals 1, while the current for the left-moving holes (function u_2^L) equals -1.

c. Decaying and growing solutions at $\varepsilon + E_F < 0$

In addition to the plane waves, Eqs. (A8) and (A9), there are two other solutions $u_1^<$ and $u_1^>$ corresponding to the eigenvalue ε_2, Eq. (A6), from the conduction band

$$u_1^< = e^{\kappa x+iqy} \begin{pmatrix} -i\,K_0/t_\perp \\ e^{\gamma} \\ -i\,K_0/t_\perp \\ e^{-\gamma} \end{pmatrix} \tag{A17}$$

and

$$u_1^> = e^{-\kappa x+iqy} \begin{pmatrix} i\,K_0/t_\perp \\ e^{-\gamma} \\ i\,K_0/t_\perp \\ e^{\gamma} \end{pmatrix}. \tag{A18}$$

The normalization in Eqs. (A17) and (A18) does not play any role and we just set it equal to unity. The parameters κ and q can be written in the form

$$\kappa = K_0 \cosh\gamma, \quad q = K_0 \sinh\gamma. \tag{A19}$$

d. Decaying and growing solutions at $\varepsilon + E_F > 0$

In this region of parameters there are growing and decaying wave functions that correspond to ε_4 from Eq. (A7) and belong to the valence band. We write the growing $u_2^<$ and decaying $u_2^>$ functions as

$$u_2^< = e^{\kappa x+iqy} \begin{pmatrix} i\,K_0/t_\perp \\ e^{\gamma'} \\ -i\,K_0/t_\perp \\ -e^{-\gamma'} \end{pmatrix} \tag{A20}$$

and

$$u_2^> = e^{-\kappa x+iqy} \begin{pmatrix} -i\,K_0/t_\perp \\ e^{-\gamma'} \\ i\,K_0/t_\perp \\ -e^{\gamma'} \end{pmatrix}. \tag{A21}$$

The parameters κ and q can be written in the form

$$\kappa = K_0 \cosh\gamma', \quad q = K_0 \sinh\gamma'. \tag{A22}$$

e. Relations between the variables α,α' and γ',γ

The variables α, α', γ, and γ' are not independent because the component q parallel to the interface is everywhere the same. Comparing Eqs. (A13) and (A22), we come to the relation

$$\sin\alpha = \sinh\gamma', \tag{A23}$$

while the comparison of Eqs. (A15) and (A19) leads to

$$\sin\alpha' = -\sinh\gamma. \tag{A24}$$

3. Transmission $t_{21}(\varepsilon)$, $t_{12}(\varepsilon)$ and reflection $r_{21}(\varepsilon)$ amplitudes

Now we calculate the transmission $t_{21}(\varepsilon)$ and reflection $r_{21}(\varepsilon)$ amplitudes that match the wave functions written on the left and on the right from the interface. Again, we consider the regions $\varepsilon + E_F > 0$ and $\varepsilon + E_F < 0$ separately. Then, the transmission amplitude $t_{12}(\varepsilon)$ can easily be obtained from $t_{21}(\varepsilon)$ through the well-known relation

$$t_{12}(\varepsilon) = t_{21}(\varepsilon) e^{i\delta(\varepsilon)}, \tag{A25}$$

where $\delta(\varepsilon)$ is a phase whose explicit value is not necessary for the calculation of the conductances using Eqs. (2.8)–(2.10).

a. Region $E_F > 0$, $\varepsilon + E_F > 0$

The scattering process at $x < 0$ includes a plane wave that is incident from the left, $u_{1U_0}^R$, and another one, $u_{1U_0}^L$, reflected from the interface. In addition, in the region $x < 0$ one has a wave that is growing with x (decaying from the interface) with the symmetry of $u_1^<$ from Eq. (A17).

After scattering off the interface one obtains an outgoing wave for $x > 0$ with the structure u_1^R, Eq. (A8), and a decaying wave with the structure $u_2^>$, Eq. (A21). We describe the scattering process for $\varepsilon + E_F > 0$ that matches these functions at the interface,

$$u_{1U_0}^R + r_{22}(\varepsilon) u_{1U_0}^L + B u_{2U_0}^< = t_{21}(\varepsilon) u_1^R + C u_2^>, \tag{A26}$$

where B and C are coefficients that have to be found by solving Eq. (A26). Actually, Eq. (A26) is a system of four linear equations and one has to find four unknown quantities, $r_{22}(\varepsilon)$, $t_{21}(\varepsilon)$, $B(\varepsilon)$, and $C(\varepsilon)$.

Writing Eqs. (A26) explicitly leads to some quite cumbersome expressions. Fortunately, these equations are simpler in the limit $U_0 \gg \varepsilon, E_F$, which is explicitly considered here. The amplitudes $t_{21}(\varepsilon)$ and $r_{22}(\varepsilon)$ can now be found rather easily. Using Eq. (3.7) we write

$$\frac{\sin\alpha(U_0)}{\sin\alpha} \simeq \sqrt{\frac{\varepsilon + E_F}{U_0}} = L(\varepsilon) \ll 1 \tag{A27}$$

to obtain in the linear approximation in α

$$\cos\alpha(U_0) = \sqrt{1 - L^2(\varepsilon)\sin^2\alpha} \simeq 1. \tag{A28}$$

We can hence approximate

$$e^{i\alpha(U_0)} \simeq 1 + i\,L(\varepsilon)\sin\alpha, \quad e^{\gamma(U_0)} = 1 + L(\varepsilon)\sinh\gamma, \tag{A29}$$

and simplify Eqs. (A26) with the help of the relations (A27)–(A29). We solve these equations and arrive at the following expression for the transmission coefficients $t_{21}(\varepsilon)$

and $r_{22}(\varepsilon)$:

$$t_{21}(\varepsilon) = \frac{2\sqrt{L(\varepsilon)\cos\alpha}\cosh\gamma'}{\cos\alpha\cosh\gamma' + i\sin\alpha\sinh\gamma'}, \tag{A30}$$

and

$$r_{22}(\varepsilon) = 1 - \frac{2L(\varepsilon)\cosh\gamma'}{\cos\alpha\cosh\gamma' + i\sin\alpha\sinh\gamma'}. \tag{A31}$$

Using Eq. (A27) we rewrite Eqs. (A30)– and (A31) in a more compact form,

$$t_{21}(\varepsilon) = 2\sqrt{L(\varepsilon)\cos\alpha(1+\sin^2\alpha)}\exp[-i\Phi(\alpha)], \tag{A32}$$

with $\Phi(\alpha)$ introduced in Eq. (3.3).

Since the angle $\Phi(\alpha)$ varies in the interval

$$0 < \Phi(\alpha) < \pi/2, \tag{A33}$$

we obtain for the reflection coefficient

$$r_{22}(\varepsilon) = 1 - 2L(\varepsilon)\sqrt{\left(1+\sin^2\alpha\right)}\exp\left[-i\Phi(\alpha)\right]. \tag{A34}$$

The unitarity condition immediately follows from Eqs. (A32) and (A34) in the limit (A27),

$$|t_{21}(\varepsilon)|^2 + |r_{22}(\varepsilon)|^2 = 1. \tag{A35}$$

b. Region $E_F > 0$, $\varepsilon + E_F < 0$

In the region $E_F > 0$, $\varepsilon + E_F < 0$ matching the wave functions at $x = 0$ results in the equation

$$u^R_{1U_0} + r_{22}(\varepsilon)u^L_{1U_0} + B(\varepsilon)u^<_{2U_0} = t_{21}(\varepsilon)u^R_2 + C(\varepsilon)u^>_1. \tag{A36}$$

Using the same approximation (A27)–(A29) and proceeding in the same way as for $\varepsilon + E_F$, one comes with the help of Eq. (A24) to the following result for the transmission amplitude:

$$t_{21}(\varepsilon) = -2\sqrt{L(\varepsilon)\cos\alpha'}\sin\alpha'\exp[i\Phi(\alpha')]. \tag{A37}$$

The reflection amplitude $r_{22}(\varepsilon)$ can be then written as

$$r_{22}(\varepsilon) = 1 - 2iL(\varepsilon)\cos\alpha'\exp[i\Phi(\alpha')], \tag{A38}$$

with

$$\Phi(\alpha') = -\arcsin(\sin^2\alpha'). \tag{A39}$$

Again, the unitarity condition, Eq. (A35), is fulfilled in the limit specified in Eq. (A27).

[1] A. F. Andreev, Sov. Phys. JETP **19**, 1228 (1964).
[2] C. W. J. Beenakker, Phys. Rev. Lett. **97**, 067007 (2006).
[3] P. A. M. Benistant, A. P. van Gelder, H. van Kempen, and P. Wyder, Phys. Rev. B **32**, 3351(R) (1985).
[4] V. Mourik, K. Zuo, S. M. Frolov, S. R. Plissard, E. P. A. M. Bakkers, and L. P. Kouwenhoven, Science **336**, 1003 (2012).
[5] J. R. Williams, A. J. Bestwick, P. Gallagher, S. S. Hong, Y. Cui, A. S. Bleich, J. G. Analytis, I. R. Fisher, and D. Goldhaber-Gordon, Phys. Rev. Lett. **109**, 056803 (2012).
[6] F. Amet, C. T. Ke, I. V. Borzenets, J. Wang, K. Watanabe, T. Taniguchi, R. S. Deacon, M. Yamamoto, Y. Bomze, S. Tarucha, and G. Finkelstein, Science **352**, 966 (2016).
[7] J.-D. Pillet, C. H. L. Quay, P. Morfin, C. Bena, A. Levy Yeyati, and P. Joyez, Nat. Phys. **6**, 965 (2010).
[8] H. B. Heersche, P. Jarillo-Herrero, J. B. Oostinga, L. M. K. Vandersypen, and A. F. Morpurgo, Nature **446**, 56 (2007).
[9] D. K. Efetov, L. Wang, C. Handschin, K. B. Efetov, J. Shuang, R. Cava, T. Taniguchi, K. Watanabe, J. Hone, C. R. Dean, and P. Kim, Nat. Phys. **12**, 328 (2016).
[10] K. S. Novoselov, A. K. Geim, S. V. Morozov, D. Jiang, M. I. Katsnelson, I. V. Grigorieva, S. V. Dubonos, and A. A. Firsov, Nature (London) **438**, 197 (2005).
[11] Y. Zhang, Y.-W. Tan, H. L. Stormer, and P. Kim, Nature (London) **438**, 201 (2005).
[12] P. G. De Gennes, *Superconductivity of Metals and Alloys* (Benjamin, New York, 1966).
[13] P. R. Wallace, Phys. Rev. **71**, 622 (1947).
[14] E. McCann and V. I. Fal'ko, Phys. Rev. Lett. **96**, 086805 (2006).
[15] J. Nilsson, A. H. Castro Neto, N. M. R. Peres, and F. Guinea, Phys. Rev. B **73**, 214418 (2006).
[16] T. Ludwig, Phys. Rev. B **75**, 195322 (2007).
[17] G. E. Blonder, M. Tinkham, and T. M. Klapwijk, Phys. Rev. B **25**, 4515 (1982).
[18] C. J. W. Beenakker, Rev. Mod. Phys. **69**, 731 (1997).
[19] L. D. Landau and E. M. Lifshitz, *Course of Theoretical Physics* (Pergamon Press, Oxford, UK, 1977), Vol. 3.